Original Paper

Landslides
DOI 10.1007/s10346-023-02090-y
Received: 1 November 2022
Accepted: 13 May 2023

Francisco Gutiérrez · Jorge Sevil · Piotr Migoń

Landslides in the Remolinos gypsum escarpment (NE Spain): controls imposed by stratigraphy, fluvial erosion, and interstratal salt dissolution

Abstract Dissolution of karst rocks (evaporites and carbonates) can cause significant mechanical weakening, but its preparatory role for landslide development has been scarcely explored. Fluvial valleys carved in gypsum bedrock typically display prominent escarpments with numerous landslides and perched valleys indicative of rapid retreat rate. The stratigraphic and cartographic analysis of the 37-km-long Remolinos gypsum escarpment in the Ebro Valley (NE Spain) reveals that landslide types are controlled by the lithological succession: (1) rotational slides in sections with mudstones and marls at the base; (2) rock-slope collapses (massive rock-falls) where the cliff includes halite packages at the foot; and (3) relatively small rock-falls and topples being the main failures affecting cliffs entirely made by gypsum. Fluvial undercutting by the highly mobile Ebro River is the main process that controls the spatial and temporal distribution of slope instability. Geomorphic and chronological evidence supports that the abandonment in 1574 of the El Castellar village was at least partially motivated by a shift in the river channel toward the escarpment and the consequent landslide activity. Several lines of evidence support the concept whereby interstratal salt dissolution (halite and glauberite), here designated as subsurface solutional undermining, play a significant preparatory role for landslide development: (1) dissolution of salt close to the scarp by the inward advance of dissolution fronts and subsidence of the overlying strata; (2) collapsed fault blocks with no offset across the grabens; and (3) brine seepages and extensive efflorescences and precipitates of Na-sulfates and halite.

Keywords Evaporite karst · Solutional undermining · Scarp retreat · Rotational slide · Rock collapse · Hanging valley

Introduction

Dissolution of karst rocks (evaporites, carbonates) may play a significant role in slope instability by the following: (1) reducing the mechanical strength of the rocks and potential failure planes; (2) causing the downward settlement of slope-forming materials above cavities and dissolution zones; and (3) oversteepening the slopes by subsidence acting at their foot. Various karst-related processes can lead to mechanical weakening, including the solutional enlargement of discontinuity planes (e.g., bedding, joints), the creation of cavities and conduit networks associated with potential failure planes, and the gravitational deformation of the rocks induced by subsurface dissolution (subsidence). In some slope movements associated with soluble formations, the vertical displacement component may be related to both landsliding and dissolution-induced subsidence. The rate and impact of these processes largely depend on the type of karst rocks. At one end of the spectrum, karstification of carbonate rocks is relatively slow and typically acts differentially, guided by discontinuity planes. At the other end, the dissolution of salt formations can be extremely rapid and commonly occurs through the migration of dissolution fronts, like the melting of an ice block (De Waele and Gutiérrez 2022).

Despite the potential significant contribution of karst processes to some slope movements, this issue has been scarcely explored and is often overlooked. Several papers document some association between dissolution processes and landsliding, although in most cases incidentally. In a Triassic evaporite karst of northern Germany, Reuter et al. (1977) illustrated landslides induced by subsidence at the foot of oversteepened slopes. Rovéra (1993), using hydrogeochemical data, demonstrated the influence of subsurface dissolution of Triassic gypsum on the development of the 10 Mm^3 Friolin landslide (Alps of Savoie, France), affecting the overlying gabbro and schist rocks in the hanging wall of a thrust. Anson and Hawkins (2002) found that dissolution of detrital calcite and gypsum in a Jurassic claystone unit contributes to reduce the shear strength of the sliding surface in the translational Soper's Wood landslide, Bath, England. At Malbun village, Liechtenstein, Seijmonsbergen and de Graff (2006), based on geomorphological mapping and electrical resistivity tomography data, inferred local landslide activity enhanced by gypsum karst. Chigira et al. (2010) documented that a significant proportion of the landslides triggered by the 2008 Mw 7.9 Wenchuan earthquake, China, occurred in karstified carbonate cliffs, with rock mass strengths significantly reduced by dissolution along discontinuity planes. In Mallorca Island, Spain, Mateos et al. (2018) reported that the development of a large rock spread in a limestone coastal cliff underlain by Triassic evaporites is favored by deep-seated gypsum dissolution. Zhang et al. (2018) reported that the development of the 2009 Jiweishan rockslide-avalanche (Wulong, China) that killed 74 people was favored by local strong karstification of the carbonate bedrock, showing numerous dissolution conduits filled by residual clays. El-Haddad et al. (2021) illustrated the important role played by dissolution features and associated collapse-related deformation in the development of landslides along carbonate-rock cliffs in Egypt. Most probably, these are relict karst features developed in the past under more humid conditions (i.e., pluvials). Wang et al. (2022) incorporated a strength reduction coefficient related to karstification in the numerical modeling of the Pusa limestone cliff collapse (Nayong, China) that caused 44 fatalities.

A number of authors report on landslides and gravitational slope deformations with a significant vertical displacement component related to mass depletion by subjacent dissolution and subsidence of the overlying material. In the Western Italian Alps, Alberto et al. (2008) documented damaging deep-seated gravitational slope deformations (DSGSD) developed on competent rocks underlain by evaporites. These authors, based on geomorphic and hydrochemical evidence from springs, demonstrated that gravitational deformation in the slopes is related to the combined effect of slope instability and dissolution-induced collapse. Flow rate and hydrochemical data were used to calculate the rate of mass removal by subsurface dissolution and mean subsidence rates at a specific DSGSD. Guglielmi et al. (2000) and Jaboyedoff et al. (2011) proposed that the driving mechanism of the 55 Mm^3 La Clapiére landslide (southern Alps, France) is deep-seated dissolution of gypsum in a Triassic formation underlying gneissic rocks, both bounded by a reverse fault dipping into the slope. This interpretation is substantiated by the former authors using chemical and isotopic analyses of sulfate-rich springs located at the foot of the landslide. Active deformation in the gigantic Peracalç Range rock spread (ca. 0.9 km^3; Spanish Pyrenees), developed on a 250 m carbonate succession underlain by tectonically thickened halite-bearing Triassic evaporites, was attributed to both interstratal dissolution and lateral salt flow toward the debuttressed front of the range (Gutiérrez et al. 2012). The kilometer-scale Zenzano rock slope collapse (Iberian Chain, Spain), bounded by a gravitational normal fault 1.8 km long, occurs associated with a 475 m high erosional escarpment underlain by halite-bearing Triassic evaporites capped by a brittle sequence. Interstratal evaporite dissolution and subsidence are considered to be the main processes responsible for the formation of the Zenzano Fault and the foundered block, with a throw of around 50 m (Carbonel et al. 2013). Cianflone et al. (2018), based on spatial relationships and hydrochemical data, inferred that active halite dissolution and subsidence related to salt mines are the main triggering and sustaining factors affecting the San Leonardo landslide in Lungro village (Crati Valley, southern Italy). In the Pégairolles-de-l'Escalette rotational landslide (Langedoc Region, southern France), developed in a claystone-gypsum unit overlain by carbonate rocks, Denchik et al. (2019) inferred a temporal association between severe rainfall episodes accompanied by greater gypsum dissolution and periods of enhanced landslide activity.

Fluvial valleys carved in gypsum bedrock typically display prominent and linear gypsum escarpments. These cliffs made up of mechanically weak and highly soluble gypsum rock show intense mass movement activity. Hanging valleys and triangular facets are common landforms associated with gypsum escarpments. Although some authors have attributed them to active normal faulting (e.g., Ibáñez and Mensua 1976; Silva et al. 1988), the most common interpretation is that they are related to a rapid retreat rate that overwhelms the downcutting capability of tributary drainages (Gutiérrez et al. 1994; Guerrero and Gutiérrez 2017). Gutiérrez et al. (2008) and Guerrero and Gutiérrez (2017) presented a long list of gypsum escarpments in Spain associated with fluvial valleys carved in Cenozoic evaporites. Rock-falls from gypsum cliffs are the type of landslide that have caused the largest number of fatalities in Spain. For instance, several events occurred in in 1856, 1874, 1903, and 1946 in Azagra village, located at the foot of an escarpment carved in Paleogene evaporites in the Ebro valley, killed 11, 100, 1 and 2 people, respectively (Gutiérrez et al. 2008 and references therein). In 1988, a rock-fall caused one fatality in Calatayud town, located at the foot of the Jalón River escarpment. Other remarkable examples of gypsum escarpments include the Salt River escarpment in Devonian evaporites (Alberta, Canada; Tsui and Cruden 1984); the Eagle River escarpment in Carboniferous formations (gypsum village, Colorado, USA); the Ure River in Permian gypsum (Ripon, UK; James et al. 1981); the Sylva River valley, carved in Permain rocks (fore-Ural region, Russia; Andrejchuk and Klimchouk 2002); or the Kızılırmak River in Oligocene evaporites (Sivas, Turkey; Gökkaya et al. 2021). Despite the importance of landslides in gypsum escarpments from the hazard and geomorphic perspective, to our knowledge, there are no studies published in the international literature including cartographic inventories. This work analyses slope instability in the 37-km-long and 190-m-high Remolinos escarpment in the Ebro Valley, which is one of the most remarkable gypsum escarpments worldwide, including highly soluble halite and glauberite beds. The main objectives of the investigation include: (1) Unravel the role played by landsliding and dissolution of landslide deposits in the development of gypsum escarpments in fluvial valleys, and the associated perched valleys indicative of rapid retreat. (2) Illustrate the impact of subsurface dissolution of evaporites (subsurface solutional undermining) on the development of landslides using geomorphic, stratigraphic, structural, and hydrochemical data. This is most probably a significant, albeit overlooked process, considering that evaporites occur in around 10% of the ice-free continental surface and that they are inevitably affected by dissolution, given their high solubility. (3) Scrutinize the potential role played by fluvial dynamics and the associated slope instability on the enigmatic abandonment of El Castellar village.

Geological and geomorphological setting

The analyzed gypsum escarpment and the associated landslides are located in the central sector of the Ebro Cenozoic Basin, which is the southern foreland basin of the Pyrenees (Pardo et al. 2004). Here, the continental sedimentary fill of the basin has been dissected longitudinally by the NW–SE-oriented Ebro River (Fig. 1). The long-term entrenchment and NE-migration of this fluvial system has generated a markedly asymmetric valley, with a stepped sequence of fluvial terraces on the SW margin, and a prominent gypsum escarpment on its opposite side (Gutiérrez et al. 1994; Guerrero and Gutiérrez 2017). The so-called Remolinos escarpment, which is the focus of this work, extends along 37 km from Tauste town to Juslibol village, upstream of Zaragoza city (Fig. 1).

Two main lacustrine formations are exposed in the Remolinos escarpment, from base to top (Quirantes 1978) (Fig. 2): (1) the evaporitic Zaragoza Formation; and (2) the carbonate Alcubierre Formation. Pérez-Rivarés et al. (2004, 2018), based on magnetostratigraphic studies carried out in the limestone-capped mesas located north of the Remolinos escarpment, known as Montes de Castejón, dated the boundary between both formations at 16.1 Ma (Fig. 2), and the top of the preserved carbonate sediments at 14.3 Ma. According to deep borehole data, the Oligo-Miocene evaporitic Zaragoza Formation has a total thickness of around 600 m, and only the upper part of the succession is exposed at the surface (Torrescusa and Klimowitz 1990). This formation, in non-weathered zones beneath the surface, consists of anhydrite, halite, and glauberite with intercalations of mudstone and marl units. However, in outcrops, it displays secondary gypsum with intercalations of mudstones and

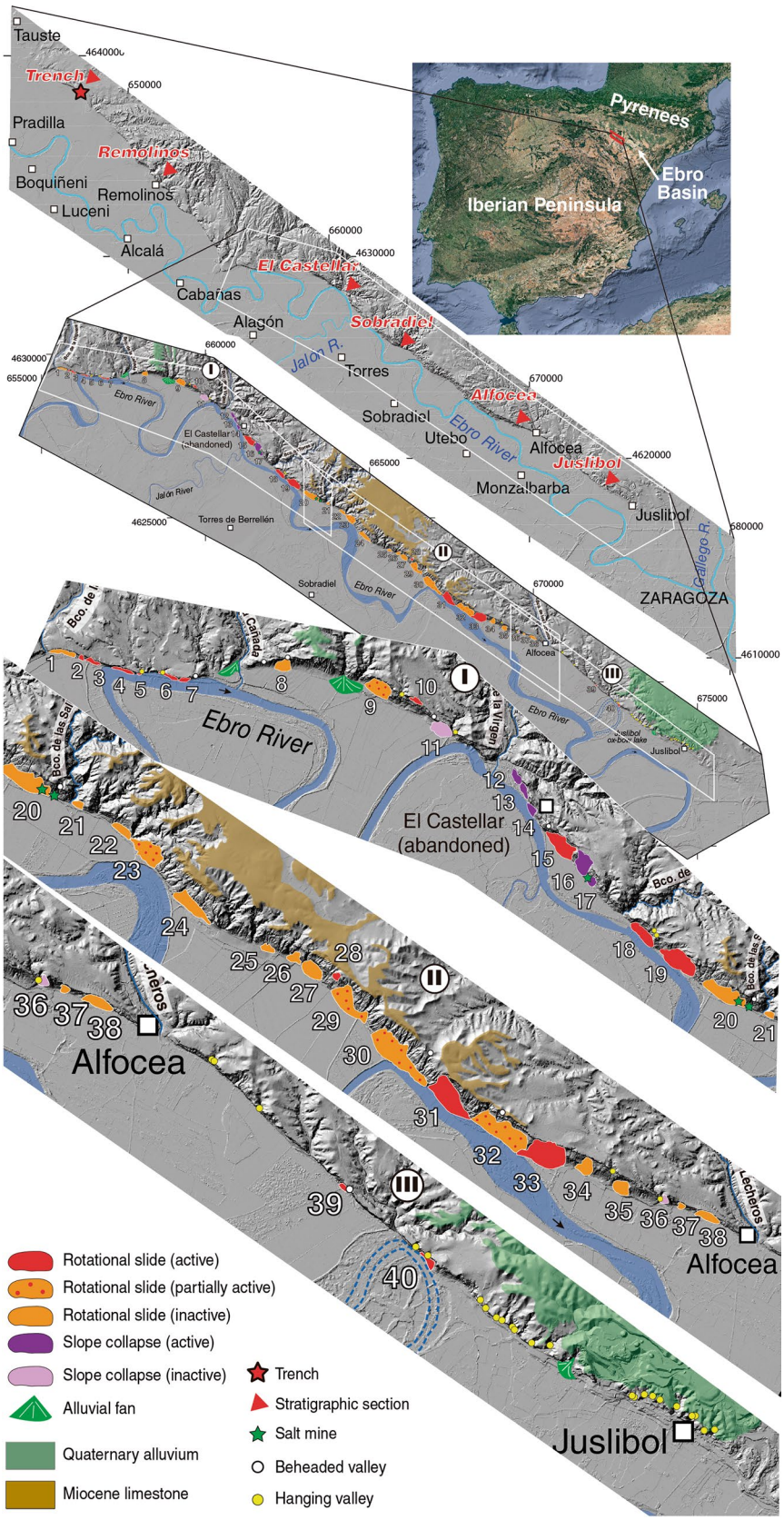

Fig. 1 Location of the Remolinos gypsum escarpment within the Iberian Peninsula (NOAA satellite image from Google Earth) and map of the escarpment showing the distribution of stratigraphic sections, inventoried landslides, hanging and beheaded valleys, and the analyzed trench. Shaded relief model generated with LiDAR data of the Instituto Geográfico Nacional

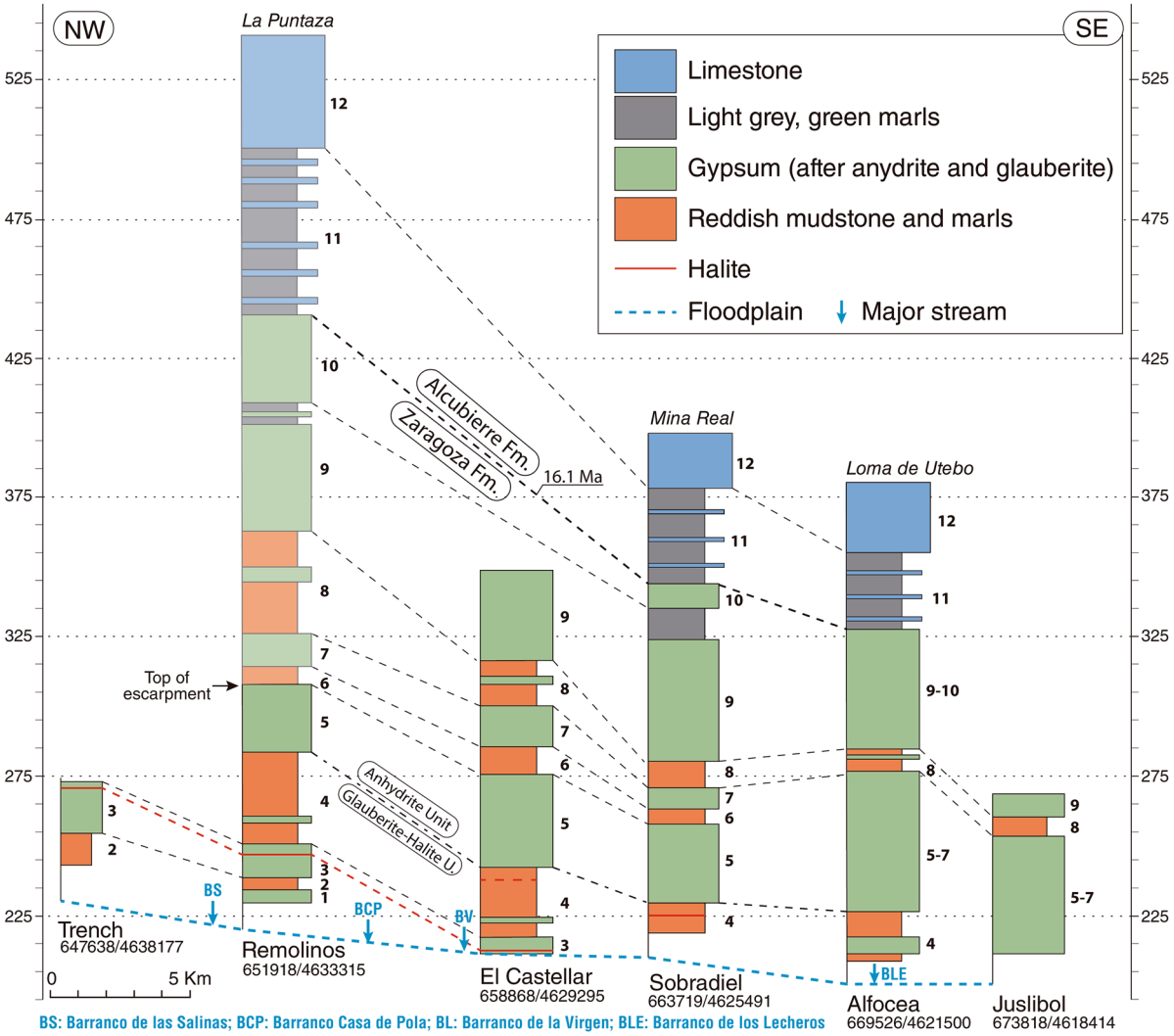

Fig. 2 Lithostratigraphic panel produced with the six stratigraphic profiles measured with a DGPS at different sections of the Remolinos escarpment (see location of stratigraphic sections in Fig. 1). The stratigraphic columns have been tied to the altitudinal scale considering the elevation at the base of the log. The position of the halite beds is based on the exploration of abandoned mines and the recognition of pointers of dissolution in the trench profile (dissolution residue, dissolution-collapse breccia). The formations and units differentiated by Quirantes (1978) and Salvany et al. (2007) are indicated, as well as the age of the boundary between the evaporitic and carbonate successions determined by magnetostratigraphic studies (Pérez-Rivarés et al. 2004, 2018)

marls. In these near-surface-weathered zones, halite beds have been dissolved and the anhydrite and glauberite have been transformed into gypsum by hydration and incongruent dissolution, respectively (Salvany 2009). Salvany et al. (2007), based on the correlation of lithological logs constructed from boreholes drilled along the Ebro Valley, differentiated four lithostratigraphic units in the Zaragoza Formation, from base to top: (1) basal marl and anhydrite unit; (2) halite unit, with halite-dominated successions us much as 75 m thick; (3) glauberite-halite unit; and (4) upper anhydrite unit. The two lower units are situated beneath the base level of erosion and remain unexposed.

In this sector of the Ebro Cenozoic Basin, the Miocene formations display a very open synformal structure with its axis located along the Ebro valley floor. The dip of the strata toward the valley is typically lower than 2°, and in some sections of the valley, the syncline shows a slight SE downstream plunge (Quirantes 1978). No evidence of tectonic faulting has been found in the escarpment, and the numerous local structures with haphazard orientations observed in the bedrock are attributed to ductile (sagging) and brittle (collapse) deformation related to interstratal dissolution of halite and/or glauberite and the subsidence of the overlying sediments (gravitational deformation).

The rocks exposed along the face of the Remolinos escarpment mostly consist of an alternation of gypsum and mudstone-marl units of the Zaragoza Formation. In the central sector, the upper part of the cliff also includes marls with limestone interbeds and a resistant limestone caprock of the Alcubierre Formation (Figs. 1 and 2). Thick pediment and terrace alluvium locally occurs at the top of

the escarpment east of Barranco de la Cañada and in Juslibol area (Fig. 1). The escarpment is dissected by transverse to highly oblique drainages, locally known as barrancos or vales. Some of these valleys are perched well above the floodplain, which functions as their base level (Fig. 1). The largest drainages show stepped sequences of inset terraces and in some cases have generated small alluvial fans at the northern valley margin (Constante et al. 2010a, b).

The Ebro River is the second longest river in the Iberian Peninsula (930 km), and has an average discharge of 231 m^3s^{-1} at the Zaragoza gauging station, with a contributing area of 40,434 km^2 and a river length of 588 km (Balasch et al. 2019). In the analyzed reach, it is characterized by a meandering channel (sinuosity of 1.6; Ollero 2010; Peña-Monné et al. 2021), which path has experienced significant changes related to meander cut-off and migration processes, mostly during flood events that essentially occur in winter and spring (Regato 1988; Ollero 2010; Gutiérrez et al. 2007, 2019). For instance, the Juslibol ox-bow lake (Fig. 1) was created by the cut-off of a meander loop during the 1961 flood (Pellicer and Yetano 1985), with an estimated peak discharge of 4130 m^3s^{-1}, considered to be the largest of the systematic gauging record that starts in 1913 (Balasch et al. 2019). The floodplain displays numerous abandoned channel sections with meandering pattern, most of which became inactive before the production of the oldest maps that depict the Ebro River, dating back to 1746 (Peña-Monné et al. 2021). The area has a semiarid climate, with a mean annual precipitation of 345 mm, an average annual temperature of 15 °C, and a potential annual evapotranspiration of 1200 mm (Cuadrat et al. 2007).

Methodology

In order to assess the potential role played by the variable lithostratigraphic succession and salt dissolution (i.e., halite and glauberite) on landslide development, a total of six stratigraphic logs were constructed at different sections of the escarpment, indicating the lithostratigraphic units exposed in the rock cliff and in higher adjacent ground to the north (Fig. 2). The data of the stratigraphic columns, with thicknesses ranging between 31 and 305 m and with an aggregate length of 862 m, have been collected in the field measuring vertically the thickness of each unit with a Differential Global Positioning System (DGPS). The logs differentiate the main packages according to the dominant lithology and their mechanical and erosional behavior (i.e., mass wasting, dissolution): resistant limestone, intermediate-resistance gypsum, weak and erodible mudstones and marls. They also indicate the stratigraphic position of the halite units exploited in the numerous mines that exist in Remolinos-El Castellar area. A number of abandoned mines were examined to describe the halite units and the effects of their near-surface interstratal dissolution.

A cartographic landslide inventory of the section of the escarpment with highest density of large landslides, between Barranco Casa de Pola and Juslibol (24 km long), was produced in a GIS environment using the following spatial data downloaded from the server of the Instituto Geográfico Nacional (IGN) (Fig. 1): (1) orthoimages from 2019 with a spatial resolution of 0.25 m; and (2) a hillshade generated with a 1-m-resolution DEM derived from ground-filtered LiDAR data from 2016. The delineation of the landslide boundaries and their categorization (e.g., typology, state of activity) was aided by field surveys and enlightening oblique aerial images taken in 2008 along the escarpment from a light aircraft. A number of morphometric parameters were extracted automatically for each landslide from the 1-m-resolution DEM using conventional GIS tools.

The gravitational deformation structures exposed in a previously existing artificial megatrench 130 m long and 40 m deep excavated across the escarpment west of Remolinos were characterized following a phased approach similar to that used in paleoseismological (McCalpin 2013) and landslide studies (Gutiérrez et al. 2010, 2012, 2015): (1) construction of a detailed stratigraphic log; (2) acquisition of numerous photographs (Canon EOS 5D Mark IV, 30.4 MP) with significant overlap (>70%) of the trench walls, placing surveying rods with known length; (3) production of scaled, high-resolution orthomosaics by Structure from Motion Photogrammetry using Agisoft Metashape Pro v.1.5.; (4) drafting of the trench logs; and (5) characterization of the deformation structures on the basis of their geometrical relationships and measurements taken from the scaled orthomosaics.

Results

Stratigraphy of the escarpment

A lithostratigraphic panel (Fig. 2) has been constructed with the six stratigraphic logs recorded at different sites along the Remolinos escarpment (see location of sections in Fig. 1). It shows the distribution of the 12 differentiated units along the escarpment and their position with respect to the valley floor. Each column has been tied to the altitudinal scale considering the elevation measured at the base of the log. The correlation lines do not represent isochrons, but time-transgressive contacts between the main lithological units. The distribution of the exposed units is influenced by two factors, in addition to the variable height of the escarpment: (1) The stratigraphic succession displays gentle apparent dips down-valley (SE) and toward the valley (SW). The fact that the overall down-valley dip is greater than the slope of the valley floor determines the exposure of progressively older units toward the northwestern sector of the escarpment. Additionally, the units occur at progressively higher elevation toward the NE, away from the escarpment, locally forming structural surfaces gently inclined toward the valley. (2) The argillaceous packages in the Zaragoza Formation show a general wedging out to the SE (down-valley) and their substitution by gypsiferous facies, reflecting deposition in more marginal versus central sectors of the evaporitic lake.

Units 1 to 10 correspond to the upper exposed part of the Zaragoza Formation (middle Miocene) (Fig. 2). We placed the boundary between the glauberite-halite and anhydrite units of Salvany et al. (2007) at the top of unit 4, which includes the uppermost halite bed mined in the area. In the Remolinos section, the glauberite-halite unit reaches an exposed thickness of 56 m, and the thickness of the anhydrite unit amounts 152 m. The exposed evaporitic succession consists of alternating units of secondary gypsum up to 50 m thick and thinner packages of mudstones and marls that may include distinctive and laterally continuous gypsum beds (e.g., unit 4). Overall, the gypsum units show an upward and downvalley thickness increase at the expense of the mudstone and marl units. The argillaceous units are typically made up of a lower section of orange to red mudstones that grade upwards into light grey to green claystones and marls with gypsum interbeds, and then into the overlying gypsum unit. The middle Miocene

Alcubierre Formation is represented by carbonate units 11 and 12 in the Sobradiel and Alfocea sections of the escarpment, with a preserved thickness of 45–50 m. At La Puntaza, NE of Remolinos, this formation reaches 100 m thick. Unit 11 is made up of light grey-green marls with interbedded limestone beds, and unit 12 consists of resistant, grey- and tan-colored limestone with abundant bioturbation and flint nodules.

Halite and glauberite units and evidence of interstratal dissolution

The lower exposed units corresponding to the glauberite-halite unit of the Zaragoza Formation defined by Salvany et al. (2007) (units 1 to 4 in Fig. 1) include economically valuable packages of halite (NaCl) and glauberite ($CaNa_2(SO4)_2$). Boreholes carried for sodium sulfate exploration south of Zaragoza city revealed a glauberite-rich succession 100 m thick (i.e., glauberite-halite unit) with glauberite packages in the subsurface us much as 30 m thick (Salvany 2009). Halite beds have been exploited by underground mines in Remolinos area over more than one millennium (Calvo 2001). The main exploited halite package is situated within the gypsum/glauberite unit 3, at approximately 4 m below the top of the unit. According to borehole data (Mina Real borehole; Ibérica de Sales pers. comm.), the halite package is 8.7 m thick and is underlain by a section 17 m thick dominated by macrocrystalline glauberite with halite cement (García-Veigas et al. 1994). This glauberite succession grades into secondary gypsum toward the surface (incongruent dissolution), which locally displays pseudomorphic gypsum after glauberite, showing the typical monoclinic prisms of the latter mineral. Excellent examples of these crystals can be observed in the analyzed trench located west of Remolinos.

The examination of abandoned mines (see location in Fig. 1), together with the construction of the stratigraphic logs, revealed that some mines in the El Castellar and Sobradiel sections of the escarpment used to exploit a stratigraphically higher halite seam situated within the mudstone and marl unit 4, at around 4–5 m below its top. This is the case of the Carabineros mines, where the excavated salt reaches 3 m in thickness (30 T 663510E 4625519N and 663175E 4625629N). The Torres de Berrellén mine (30 T 661664E 4626991N), which entrance has been recently buried by landslide deposits, was most probably also excavated in this halite bed within unit 4.

Exposures of halite and glauberite are extremely rare due to their high solubility, with equilibrium solubilities in pure water and normal conditions of 356 gr/L and 118 gr/L, respectively, in contrast to the solubility of gypsum of 2,6 gr/L (De Waele and Gutiérrez 2022). In the abandoned mines, it can be observed that the halite packages rapidly pinch out toward the surface, grading into a dissolution residue overlain by deformed supra-salt strata (Fig. 3A). The leakage of the ductile salt, unaffected by fractures, progresses through the lateral and vertical migration of dissolution fronts (Warren 2016; De Waele and Gutiérrez 2022). The dissolution residue typically consists of massive dark brown clay with calcium sulfate nodules, representing the less soluble components of the salt deposit; dark grey clay partings and anhydrite nodules embedded in the salt. The dissolution of the halite package, as much as 8.7 m thick and with a purity of > 80%, involves a substantial near-surface condensation of the stratigraphic succession. This implies that thickness measurements at the surface provide minimum estimates. The overlying strata often display local passive-bending folds with meter-scale amplitude and rather random orientations attributable to differential interstratal dissolution and sagging subsidence. The supra-salt gypsum strata of unit 3 locally have been transformed into a dissolution-collapse breccia, as can be observed in the trench section. Less commonly, the sediments overlying the halite beds display evidence of brittle deformation, including collapse structures bounded by ring gravitational faults and transtratal breccia pipes (Fig. 3B).

Saline efflorescences provide evidence of current interstratal salt dissolution within the rock mass, seepage of the resulting brines toward the surface, and evaporative precipitation. In the trench section, the exposure of unit 2 consisting of reddish mudstone with interbedded glauberite/gypsum beds displays extensive and thick white efflorescences attributable to sodium sulfates (i.e., glauberite and mirabilite) with powdery texture and locally showing glomerular to coralloid morphologies (Fig. 3C). It seems that these efflorescences of sodium sulfate are best developed in recently excavated or rapidly eroding rock faces, where primary glauberite is still present close to the surface. These type of efflorescences are used in some Cenozoic basins as pointers of concealed glauberite units (e.g., Ordóñez 2022). Halite precipitates with popcorn and stalactite morphologies associated with brine seepages are relatively common in rock walls excavated by streams in the halite-bearing unit 3 (e.g., Barranco de las Salinas, Barranco de Lora) (Fig. 3D). The mass depletion caused by the interstratal dissolution of the extremely soluble halite and glauberite units contributes to reduce the mechanical strength of the overlying sediments (i.e., solutional undermining) and causes their downward displacement (i.e., subsidence).

Landslide types, activity, distribution, and geomorphic effects

A total of 40 relatively large landslides have been mapped in the 24-km-long section of the escarpment between Barranco Casa de Pola and Juslibol village (Fig. 1). In addition, numerous small rock-falls and rock-topples occur along the cliff, but these have not been represented on the map. Two types of slope movements have been differentiated in the map: 33 rotational slides, and 7 large, short-runout rock-falls, here designated as rock-slope collapses. In this work we use the term "rock-slope collapse" to designate massive, short-runout rock-falls in the gypsum escarpment controlled by deep-penetrating, subvertical and transtratal failure planes, typically developed in sections of the cliff affected by undermining related to subjacent salt dissolution. Table 1 includes an inventory of the mapped landslides indicating a number of attributes (type, activity, stratigraphic units affected) and morphometric parameters, including the shortest distance between the landslide boundary and the river channel.

The rotational slides occur associated with stretches of the escarpment where the presence of mudstone and marl units allows for the development of curved sliding surfaces. Two relatively small slumps are perched well above the valley floor (landslides 10 and 28), affecting the mudstone unit 8 and the overlying ones (Figs. 1, 4 and Table 1). The slumped bodies are mostly elongated and parallel to the escarpment, with average width and length of 288 m and 124 m, respectively, yielding a mean width to length ratio of 2.3.

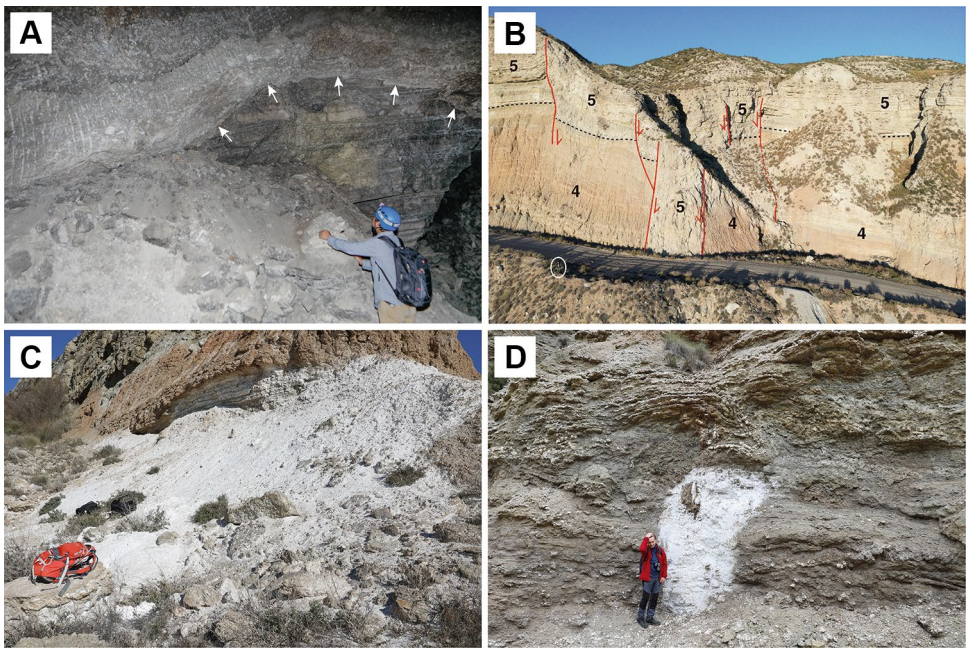

Fig. 3 Images showing evidence of interstratal salt (halite, glauberite) dissolution and gravitational deformation of the overlying sediments. **A** Sharp lateral and vertical contact (arrows) between the halite package on unit 3 and a dissolution residue made up of clay and calcium sulfate nodules. The contact corresponds to a dissolution front that progresses downwards and laterally into the salt body. Note the monoclinal fold draping the sloping dissolution front. **B** Transtratal collapse structure in Remolinos affecting units 4 and 5 with nested collapse faults and an inner breccia pipe of angular gypsum. This structure is probably related to differential dissolution of the 8.7 m thick halite bed situated in the upper part of unit 3. Ellipse indicates person for scale. **C** Extensive white efflorescence of sodium sulfates (glauberite, mirabilite) in the lower part of unit 2 exposed in the Trench. Here, the recently excavated unit 2 includes gypsum beds with monoclinic crystals corresponding to pesudomorphic secondary gypsum after glauberite. **D** Halite efflorescence associated with a seepage point in an exposure of the halite-bearing unit 3 at Barranco de las Salinas. Note synsedimentary box synform in the overlying gypsum beds (upper layers are not folded)

The largest rotational slides occur in the central sector (landslides 30 and 32), with areas of around 100,000 m² and widths of about 700 m (Table 1 and Fig. 4C). The head scars of these landslides typically display a vertical cliff made up of gypsum, or limestone and marls of units 11 and 12. Here, unloading cracks, rock-falls and topples are common. The slid mass, with relatively low mechanical resistance, is typically transformed by internal deformation into a chaotic megabreccia of gypsum blocks with reddish mudstones. Large blocks with bedding dipping into the slope are commonly observed. The upper part of the back-tilted landslides typically displays a conspicuous bench underlain by debris derived from the head scar. Some landslides show two benches related to multiple retrogressive or progressive failures. The lower part of some slumps associated with the river channel have been trimmed by fluvial erosion, exposing the sliding surface and eventually inducing partial reactivations in the landslide toe (Fig. 4).

The slope collapses (short-runout massive rock-falls) mostly occur around the abandoned village of El Castellar (Figs. 1 section I, 5, 6, 7). They reach around 17,000 m², have average width and length of 185 m and 117 m, respectively, and a mean width to length ratio of 1.6, lower than that of the rotational slides (Table 1). These slope movements typically display nearly vertical head scars and a steep and high-relief cone-shaped accumulation of gypsum megabreccia with muddy matrix (Figs. 5A and 6). The movement of the collapsed material is dominated by vertical displacement with limited runout, and evidence of back-tilting is lacking. The slope collapses associated with the river channel may show a trimmed toe and internal secondary failures expressed as downhill-facing scarps within the landslide deposits (Figs. 6 and 7).

A total of 15 rotational slides out of 33 are considered fully active, with evidence indicating that the whole slide mass is affected by ongoing or very recent displacement (e.g., fresh head scar, no evidence of degradation) (Figs. 1, 4A and Table 1). Five slumps show evidence of partial activity, affecting either the head scar (e.g., significant slumps; landslides 9, 23, 29), or the lower part (landslides 30, 32) (Fig. 4B). The average distance to the channel of the active and partially active rotational slides (shortest distance between landslide polygon and channel margin) is 195 m (84 m excluding the perched landslides), while the mean distance for the 13 inactive ones is 528 m. Regarding the rock-slope collapses, five out of seven are classified as active, with an average distance to the river channel of 144 m, whereas the two inactive ones show a mean distance of 331 m. Overall, active and partially active landslides, regardless of their type, tend to be associated or close to the river channel, with an average distance of 184 m, as opposed to the mean distance of 501 m for the inactive slope movements.

The mapped section of the escarpment shows a high density of landslides, with a linear density of 44.3%, considering the total width of the slope movements and the length of the scarp. Between Alfocea village and the Juslibol ox-bow lake there are only two small

Table 1 Landslide inventory, indicating the type of slope movement (*R*, rotational; *SC*, slope collapse; *P*, perched), the state of activity (*I*, inactive; *A*, active; *PA*, partially active; *h*, activity in head; *f*, activity in foot), the associated damage, and a number of morphometric parameters, including distance to the river channel. Mean values for the rotational landslides and slope collapses are indicated at the bottom of the table. Height of slope refers to the local relief from the crest of the escarpment to the valley floor

Code	Type	Activity	Damage	Distance to channel (m)	Units affected	Area (m^2)	Length (m)	Width (m)	Height of slope (m)	Height of deposit (m)
1	R	I		337	4to5	14,008	54	313	50	37
2	R	A		229	4to5	3114	57	66	50	38
3	R	A		32	4to5	7129	57	188	46	44
4	R	A		0	4to5	8402	44	269	50	29
5	R	A		0	4to5	894	26	55	37	19
6	R	A		0	4to5	7483	49	243	49	44
7	R	A		0	4to5	5285	56	141	49	44
8	R	I		370	4to7	20,145	154	194	73	65
9	R	PA (h)		644	4to9	43,511	177	316	120	111
10	R (P)	A		534	8to9	7002	57	173	123	44
11	SC	I		79	3to9	31,436	157	265	101	83
12	SC	A		64	3to7	12,181	88	194	75	45
13	SC	A		17	3to9	10,124	80	197	93	44
14	SC	A		0	3to9	9978	88	183	107	70
15	R	A	Track, hermitage	41	3to9	53,812	166	434	115	100
16	SC	A		321	3to9	37,565	211	237	111	111
17	SC	A	Mine	317	3to7	9731	103	114	130	75
18	R	A		0	4to9	34,293	114	367	121	54
19	R	A		0	4to9	73,937	228	490	119	108
20	R	I		120	4to11	70,261	188	554	148	107
21	R	I		586	4to7	7064	73	131	60	40
22	R	I		221	4to9	15,334	81	231	132	42
23	R	PA (h)		19	4to9	52,171	244	379	112	112
24	R	I		51	4to9	41,425	140	477	164	66
25	R	I		924	4to5	8612	76	153	136	30
26	R	I		1186	4to10	11,335	122	155	118	75
27	R	I		998	4to10	27,485	143	248	133	68
28	R (P)	A		938	8to10	5213	81	86	158	69
29	R	PA (h)		414	4to10	57,422	202	468	169	123
30	R	PA (f)	Road	0	4to12	110,878	238	746	182	95
31	R	A		0	4to12	79,656	210	528	173	129
32	R	PA (f)		0	4to12	97,612	192	623	159	114

Table 1 (continued)

Code	Type	Activity	Damage	Distance to channel (m)	Units affected	Area (m^2)	Length (m)	Width (m)	Height of slope (m)	Height of deposit (m)
33	R	A		0	4to10	88,820	270	495	131	131
34	R	I		348	4to10	22,692	188	181	119	99
35	R	I		455	4to10	21,439	152	195	99	63
36	SC	I		584	4to10	6204	92	104	87	67
37	R	I		610	4to7	3900	64	81	73	41
38	R	I		654	4to7	16,450	84	265	63	55
39	R	A		1042	4to7	3150	42	95	55	27
40	R	A		0	4to7	6091	61	170	59	42
Mean R				326		31,091	124	288	104	69
Mean SC				197		16,746	117	104	101	71

rotational slides (Fig. 1 section III). This is attributed to the fact that the scarp is mostly made up of competent gypsum of unit 5–7, with a small section of mudstones of unit 4 at the base of the cliff (Fig. 2). East of the Juslibol ox-bow lake, where the cliff is only composed of gypsum, no landslides have been mapped. Here, the evolution of the scarp is dominated by relatively small rock-falls and rock-topples controlled by unloading cracks (Pellicer et al. 1984). A similar situation is found in the section of the escarpment between Tauste town and Barranco Casa de Pola, not covered by the map. Here, the base of the scarp is made up of the competent gypsum/glauberite unit 1, inhibiting the development of slumps. Moreover, the river channel is located at significant distance from the escarpment. Rotational slides occur all along the escarpment between Alfocea and Barranco de Casa de Pola, mainly controlled by the mudstone and marl unit 4 at the base or lower part of the cliff (Fig. 1 and Table 1). The largest slumps occur between Barranco de Torres and Alfocea, where the escarpment reaches its greatest height (ca. 180 m) because of the presence of a limestone caprock of the Alcubierre Formation (unit 12) (Fig. 4C). The graph of Fig. 8 (slope height versus area of the rotational slides) shows that the 15 rotational slides with areas greater than ~20,000 m^2 occur at sites where the local relief of the escarpment exceeds ~100 m. The data are distributed above a sloping bound suggesting the need for minimum slope height values for the development of slumps of a certain size. Six slope collapses (landslides 11, 12, 13, 14, 16, 17) out of seven are concentrated in a 2.6 km section of the escarpment around the Barranco de la Virgen and the abandoned village of El Castellar (Fig. 5B). Here, the basal part of the cliff includes the 8.7 m and 3 m thick halite packages of units 3 and 4, respectively, suggesting some causal relationship (Figs. 6 and 7).

The mapped gypsum escarpment displays numerous perched valleys. In our map we have differentiated two different types (Fig. 1): (1) 31 hanging valleys corresponding to streams flowing toward the Ebro Valley that terminate abruptly at the escarpment, with the thalweg often perched tens of meters above the valley floor (Fig. 4B, C); and (2) 9 beheaded valleys, where the head of streams flowing away from the face of the cliff have been truncated by the retreat of the escarpment. The latter valleys often show drainage reversals, with sections sloping toward the Ebro Valley that used to drain in the opposite direction. Hanging valleys essentially form in low-order streams (Strahler's system) with small catchment areas. Interestingly, 23 out of 31 of the mapped hanging valleys occur between Alfocea and Juslibol villages, where the number of landslides is very limited and the cliff is essentially made up of the thick gypsum package corresponding to unit 5–7 (Fig. 1III). Beheaded valleys are distributed all along the scarp and occur mostly associated with first order channels. They seem to be particularly frequent in the sections where the gypsum uplands are dissected by valleys with an oblique orientation with respect to that of the escarpment (e.g., Barranco de los Lecheros). These drainages have tributaries with favorable orientation for the development of beheaded valleys.

Landslides at the abandoned village of El Castellar

The abandoned village of El Castellar is mostly located on the slopes of a deeply entrenched and NW-directed tributary of the Barranco de la Virgen, called Barranco Conejero. Most of the ruins occur on the SE flank of the valley up to the crest of the escarpment, where remains of a Medieval castle are currently being destroyed by rock-falls and rock-topples above landslide 14 (Figs. 5 and 6). The 110 m high escarpment at El Castellar is made of an alternation of gypsum and mudstone packages, including units 3 to 9, with the odd numbers corresponding to the evaporites (Fig. 6). Unit 3, which includes the 8.7 m thick halite bed in its upper part, is largely concealed by landslide deposits, but 5–9 m of the upper part of the unit crops out at the mouth of the Barranco Conejero and the Barranco de la Virgen. The exposed section of this unit is a condensed sequence resulting from the near-surface dissolution of the halite bed. The stratigraphic log constructed at El Castellar indicates that the halite bed is situated at the basal part of the escarpment, a few

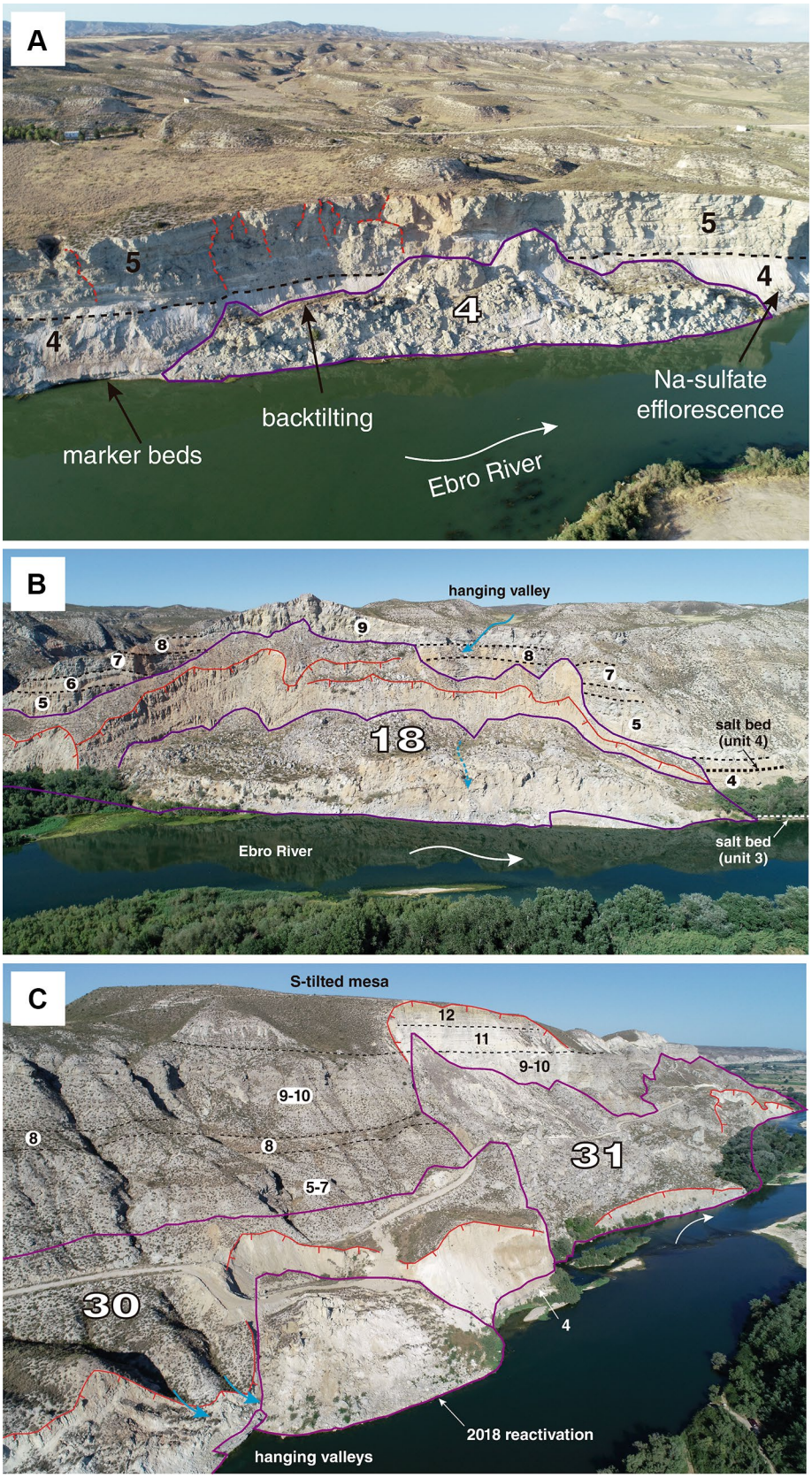
A
5
4
5
4
4
marker beds
backtilting
Ebro River
Na-sulfate
efflorescence
B
hanging valley
9
8
7
6
5
8
7
5
18
salt bed
(unit 4)
4
Ebro River
salt bed
(unit 3)
C
S-tilted mesa
12
11
9-10
9-10
8
8
5-7
31
30
4
2018 reactivation
hanging valleys

◂**Fig. 4** Images of rotational slides associated with the river channel and developed in sections where the base of the escarpment is made up of mudstone of unit 4. **A** Landslide 4 affecting units 4 and 5. Note abundant white saline efflorescences in the exposures of unit 4. **B** Landslide 18 involving units 4 to 9. This landslide, affected by fluvial undermining, shows evidence of partial activity in the lower half of the slid mass. Note hanging valley. **C** Landslides 30 (left) and 31 (right). The former shows evidence of activity in the lower part, including a slump triggered by a flood in 2016 that cut a dirt road. Landslide 31 affects units 4 to 12

meters above the normal river water level. The 25 m thick unit 4 is discontinuously exposed along the lower part of the cliff. Most probably, this unit also includes the ≥3 m thick halite bed which was mined at the El Castellar (Fig. 7) and Carabineros mines, located 1 and 3 km to the SE (Fig. 5B). Unit 9 is a rather massive gypsum package that forms the caprock of the escarpment and the foundation of the human structures of the El Castellar village lying at higher elevation. This unit, underlain by the mechanically weak mudstones of unit 8, is affected by numerous dilated cracks, many of which penetrate across the whole package. These discontinuities that guide water infiltration and dissolution control the development of meter- to decameter-scale rock-falls and rock-topples. These slope movements cause the retreat of the upper part of the cliff and the destruction of the most remarkable buildings of the village, generating a striking geomorphological-cultural landscape (Figs. 5C and 6).

At El Castellar, landslide 14 displays a nearly vertical and arcuate scar beneath unit 9 and attributable to a rock slope collapse. The cone-shaped deposit is 88 m long, 183 m wide, has a local relief of 70 m and very steep slope. The slid mass displays some internal fresh-looking secondary scars that allow differentiating four subsequent failures (Fig. 6). The cross-cutting relationships between the scars allow establishing a chronological order for their formation, from La to Ld, likely induced by fluvial erosion at the toe.

An interesting issue is whether slope instability played some role on the abandonment of El Castellar village, which in the Middle Ages, after the Reconquest, experienced significant expansion, becoming a village with hundreds of inhabitants and four churches or hermitages. According to Gascón Ricao (2007), the village was finally abandoned in 1574 because of the migration of the inhabitants toward valley floor. It is likely that natural factors played some role in the abandonment, including potential variations in the river path and destruction of human structures by landsliding. It seems reasonable to consider that in the past (i.e., the start of the Christian settlement in the 12th Century), the channel of the Ebro River was located further to the south, and the inhabitants of El Castellar used to have direct access to fertile land on the northern bank of the river. At some stage, the highly unstable river channel shifted to the foot of the escarpment, blocking direct access to crop fields in the floodplain and instigating the collapse of the escarpment by fluvial undermining. Constraining the timing of the Ebro River channel shift, and therefore the associated erosional processes (e.g., removal of the alluvial fan fed by Barranco de la Virgen, basal undermining, slope movements), is essential for assessing the potential role played by these hazards on the abandonment of the village. The timing of the shift of the river channel to the foot of the escarpment can be situated approximately by dating its geomorphic effects on the Barranco de la Virgen, situated just NW of El Castellar. Constante et al. (2010a) mapped three stepped Holocene terraces in the lower reach of the Barranco de la Virgen, just NW of El Castellar: (1) an old fill terrace ca. 14 m thick with its tread situated at 12 m above the thalweg; (2) an intermediate fill-strath terrace at 6 m above the channel with a veneer around 1 m thick inset into the deposits of the older level; and (3) a lower level represented by discontinuous deposits < 1 m thick restricted to the inner side of the meanders. The intermediate level perched 6 m used to connect with an alluvial fan on the valley margin, which has been eroded by the migration of the Ebro River toward the escarpment (Fig. 5). This geomorphic change involved a local drop in the base level of the Barranco de la Virgen, leading to the incision phase after the formation of the intermediate terrace. Constante et al. (2010a), based on Medieval structures buried by the deposit of the intermediate level in the vicinity of the La Magdalena Hermitage, tentatively date the initiation of this incision phase at around 1500 AD. This age is consistent with the hypothesis whereby the migration of the river and the associated slope instability contributed to the progressive abandonment of El Castellar village, which finished in 1574. Geomorphic evidence for the potential previous path of the river channel is provided by a well-preserved abandoned meander loop with SW-facing convexity located just north of Torres de Berrelén and around 1.2 km SW of El Castellar (Fig. 6B). An investigation in this relict channel, including boreholes with core recovery and numerical dating, would shed light on the chronology of its cut off.

The old El Castellar Hermitage, located further to the SE, was destroyed in the nineteenth century by the retreat of the headscar of landslide 15. In 1847, José Gotor, parish priest of Torres de Berrellén, reported that on the 24 of March, 1840, at 19:30, the Hermitage of El Castellar (also called Santa María del Rosario), that used to be located at the crest of the escarpment on rocks undermined by the Ebro River, collapsed together with a large landslide. The workers that witnessed the catastrophic mass movement described that it temporarily dammed the river and created a wave (i.e., impulse water wave) that ejected water and fish toward the opposite channel bank (Gascón Ricao 2007). This account suggests that the destruction of the hermitage was caused by a rock collapse in the head scar of the rotational slide 15, located next to the river channel (Fig. 5B).

Gravitational deformation at the trench site

Between Tauste and Remolinos, a megatrench was excavated across the gypsum escarpment for the construction of a water pipe connected to La Loteta Reservoir (Figs. 1 and 9). Here, the escarpment is made of units 2 and 3 (Fig. 9). The upper part of the escarpment is a flat structural surface controlled by the top of unit 3. The slope shows two flat benches at the foot of fresh-looking fault scarps with wide open fissures. The section of the escarpment with the elongated downthrown blocks extends along 290 m. The cliff and the associated gravitational structures are cut in their middle sector by a trench with a sub-perpendicular orientation (N35E) with respect to the escarpment (Fig. 9). The trench, with benched walls, is 130 m long, 55 m wide, and reaches a remarkable depth of 40 m. The stratigraphy exposed in the excavation include four subunits corresponding to unit 2 (I to IV) and four subunits of unit 3 (V–VIII), described in Fig. 9. The exposed section of unit 2 essentially consists of a lower part of glauberite beds with dark-colored marls and

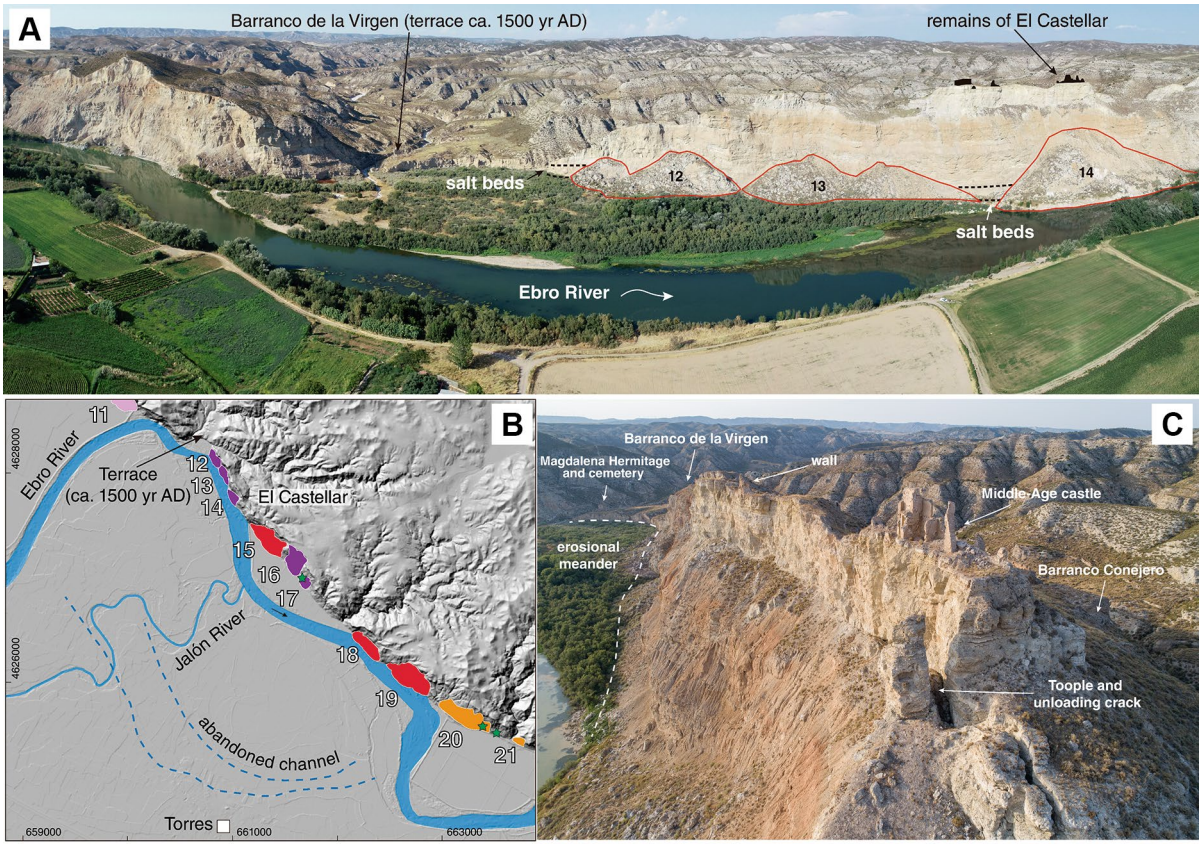

Fig. 5 Section of the escarpment associated with the village of El Castellar, abandoned in 1574. **A** View of the escarpment around El Castellar, showing the terrace of the Barranco de la Virgen (ca. 1500 year AD) trimmed by the river and the rock-slope collapses 12 to 14. These massive rock-falls occur in sections where the lower part of the cliff includes the halite-bearing units 3 and 4. **B** Excerpt of the landslide map on a shaded relief model showing the position of an abandoned channel at significant distance from the escarpment. **C** View of the destroyed castle of El Castellar, built on the gypsum unit 9 affected by rock-falls and rock-topples controlled by fractures induced by unloading and probably also subsurface solutional undermining. Barranco de la Virgen and its incised valley fill in the background

mudstones, and an upper part of reddish mudstones and marls. The ground surface at the lower part of unit 2 is covered by white Na-sulfate efflorescences up to several centimeters thick providing evidence of current glauberite dissolution and partial precipitation by evaporation. The green-grey marls with a conspicuous gypsum interbed of subunit IV constitute an excellent marker to characterize the deformation structures. Unit 3 is mostly composed of gypsum largely derived from glauberite, as reveal the abundant pseudomorphs. The upper subunit VIII is a collapse breccia related to the interstratal dissolution of the halite bed mined in Remolinos area that occurs in the upper part of unit 3 (Figs. 2 and 9).

The log of the SE wall of the trench, delineated on the orthomosaic produced by Structure from Motion Photogrammetry, shows a 50 m wide deformation zone associated with the face of the escarpment, including two keystone grabens and an intervening horst with geomorphic expression (i.e., benches and marginal fissures) (Fig. 9). To the NE of this deformation zone, the bedrock shows non-faulted beds with horizontal attitude locally affected by subvertical open fissures with limited vertical extent. The NE graben, bounded by faults F1 and F2, shows some back-tilting (ca. 5°) and an arcuate cavity related to an internal collapse attributable to subsurface glauberite dissolution. Faults F1 and F2 show throws of 4.8 and 2.3 m, respectively, and are accompanied by fissures (f1 and f2) filled by soft gypsiferous silts with angular gypsum clasts. A remarkable feature is that there is no vertical offset across the NE graben; subunit IV lies at the same elevation on both sides. Bedding in the horst, bounded by faults F2 and F3, displays a subhorizontal attitude. The SW graben is controlled by fault F3 and the antithetic fault F4 with an upward splay. The throw of fault F3 is 4.2 m, while that of F4 is 1.9 m, indicating some subsidence in the sediments SW of the graben. In fact, subunit IV shows a vertical offset of around 3 m across the two grabens. The subcircular failures designated as fault F5 correspond to small rotational slides cross-cutting fault F4 and superimposed on the SW graben. Interestingly, the sediments in the outermost section of the trench, SW of fault F4, do not show any back-tilting or internal deformation, as it would be expected in case the deformation structures would correspond to a rotational slide or a lateral spread. Overall, the trench shows differential subsidence structures expressed as downthrown fault-bounded blocks dominated by vertical displacement attributable to the lack of basal support by interstratal glauberite dissolution (subsurface solutional undermining). Evidence of active glauberite dissolution is provided by the extensive white efflorescences draping the recently created exposures of unit 2 (Figs. 3C and 9). The dissolution of the higher

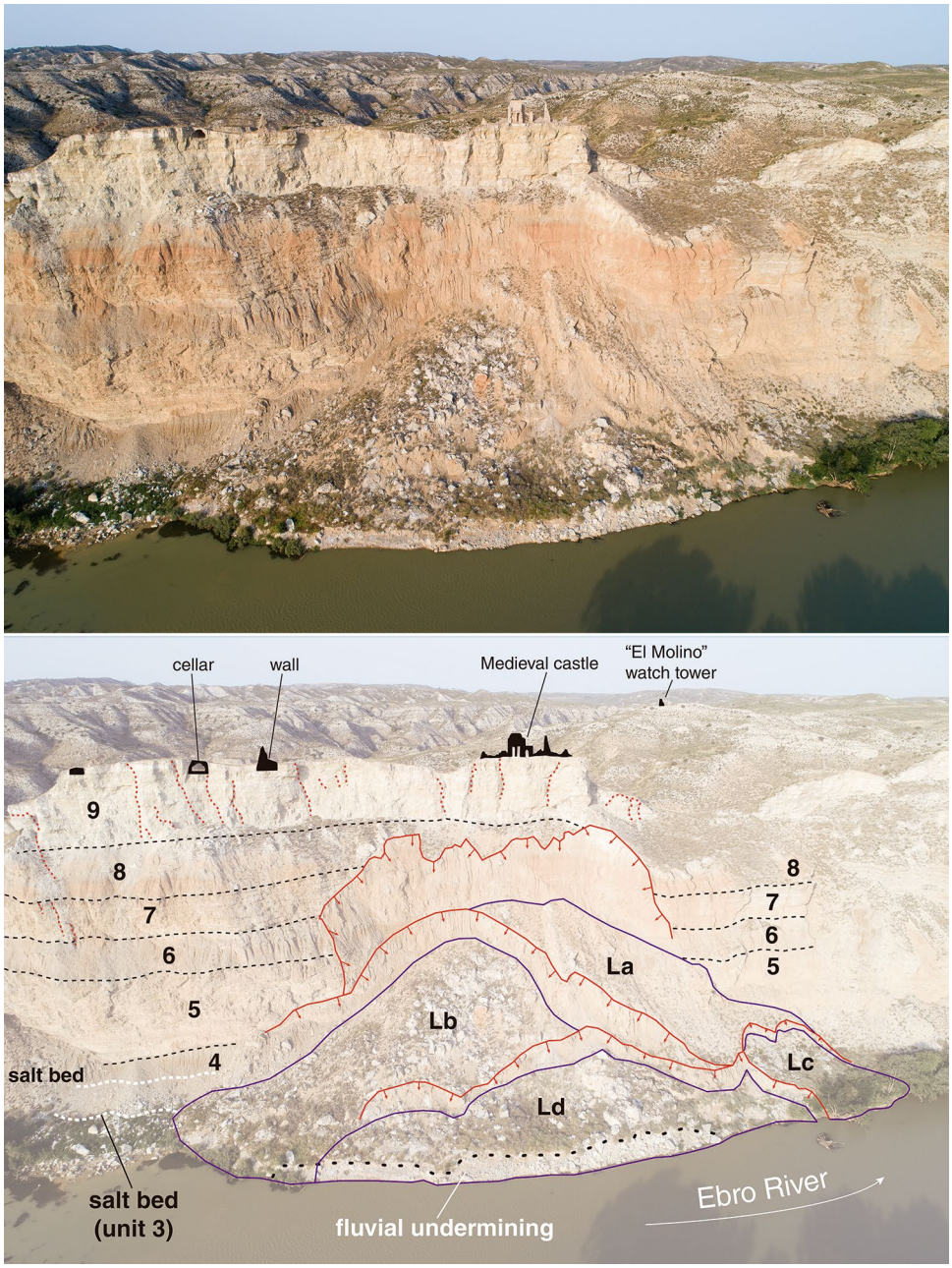

Fig. 6 Slope collapse (landslide 14) below the Medieval castle of El Castellar, affecting units 3 to 8 and undermining unit 9. The landslide deposits show internal fresh scars, which cross-cutting relationships allows establishing a chronological sequence for the secondary failures. Note position of the halite beds in unit 3 and 4, and the trimmed toe of the landslide

lying halite bed of unit 3 and the formation of the stratiform collapse breccia (subunit VIII) was older than the development of these fault-controlled collapse structures, incorporated in the downthrown blocks.

Discussion

The spatial relationships between the mapped landslides and the lithostratigraphic units (Figs. 1, 2 and Table 1) reveal that stratigraphy plays a major control on the location of landslides and their failure mechanisms. As expected, most of the rotational landslides occur west of Alfocea village, where the base of the cliff includes relatively thick mudstones and marls of unit 4 (Fig. 4). Between Alfocea and Juslibol ox-bow lake, where the thickness of unit 4 at the base of the scarp is very limited (< 5 m), there are only two small rotational slides, while slumps are absent east of the Juslibol ox-bow lake, where a competent gypsum package underlies the entire scarp. The presence of mechanically weak argillaceous sediments at the base of the escarpment allows for the development of listric failure planes, with a subvertical section above unit 4, and a curved section within unit 4, responsible for the back-tilting of the slid mass.

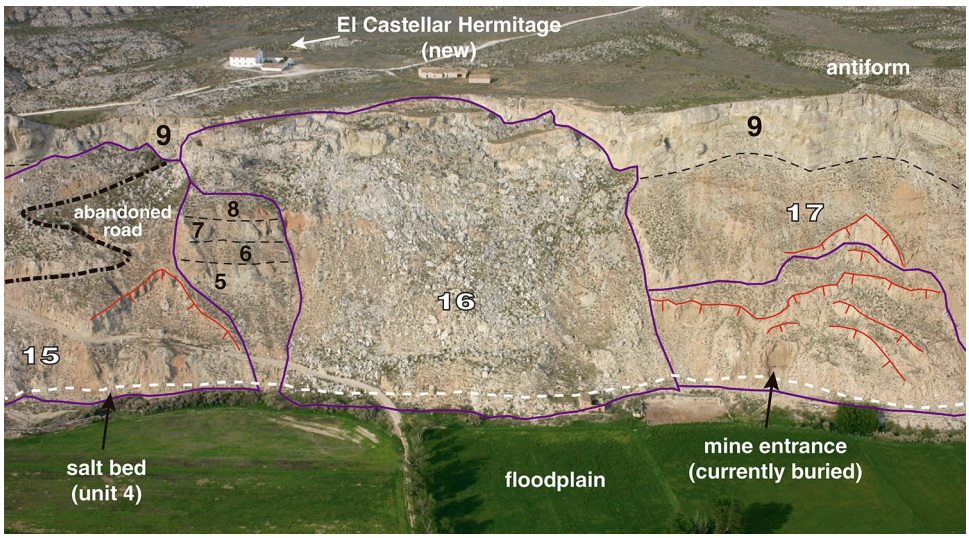

Fig. 7 Aerial view of the rotational landslide 15 and the slope collapses 16 and 17, affecting units 4 to 9. Note the position of halite bed of unit 4 at the foot of the scarp and the entrance of the Torres de Berrellén mine in landslide 17. The active landslide 15 damaged the old road to El Castellar Hermitage

The large short-runout rock falls designated as slope collapses are essentially restricted to the section of the escarpment where two halite beds around 9 m and 3 m thick occur at the base of the cliff (Figs. 5, 6 and 7). This spatial association suggests that interstratal salt dissolution (halite and probably glauberite) near the face of the scarp and the consequent mechanical weakening of the overlying sediments related to gravitational deformation plays a significant preparatory role in the development of this type of landslides.

The cartographic work shows that fluvial undercutting by the meandering Ebro River channel, which path has experienced continuous changes, is the main triggering factor for the development and reactivation of landslides (Fig. 1 and Table 1). The landslides in the 24-km-long mapped section of the escarpment show a much higher spatial density (linear density of 44%) than in the 13-km-long section between Tauste and Barranco Casa Pola, where the river channel does not interact with the scarp. The coupling

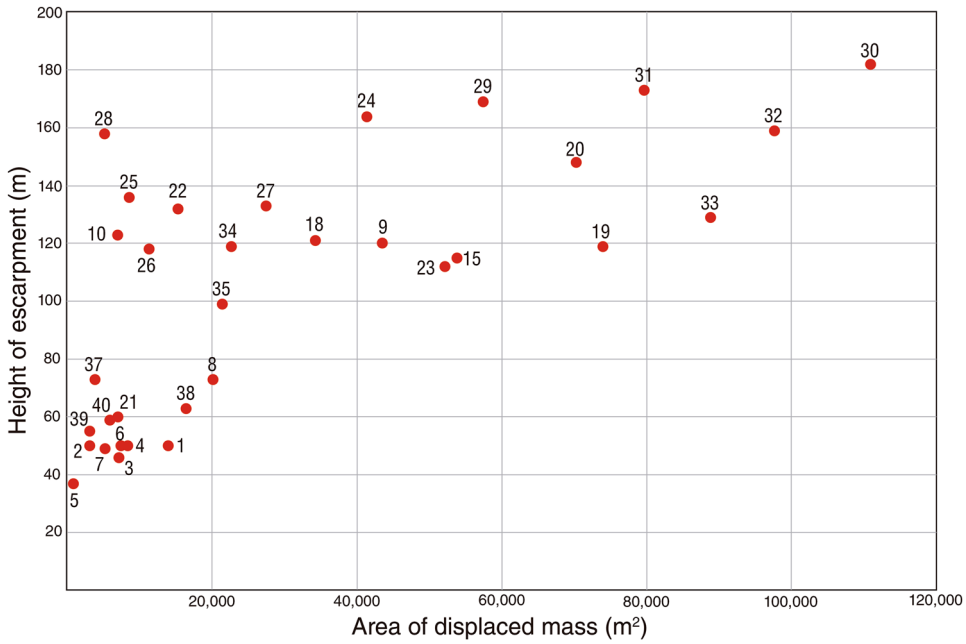

Fig. 8 Graph showing the overall direct relationship between the height of the escarpment and the area of the rotational slides (displaced mass), as well as a lower bound in the distribution of the data suggesting the need for a minimum slope height for the development of landslides of a certain area

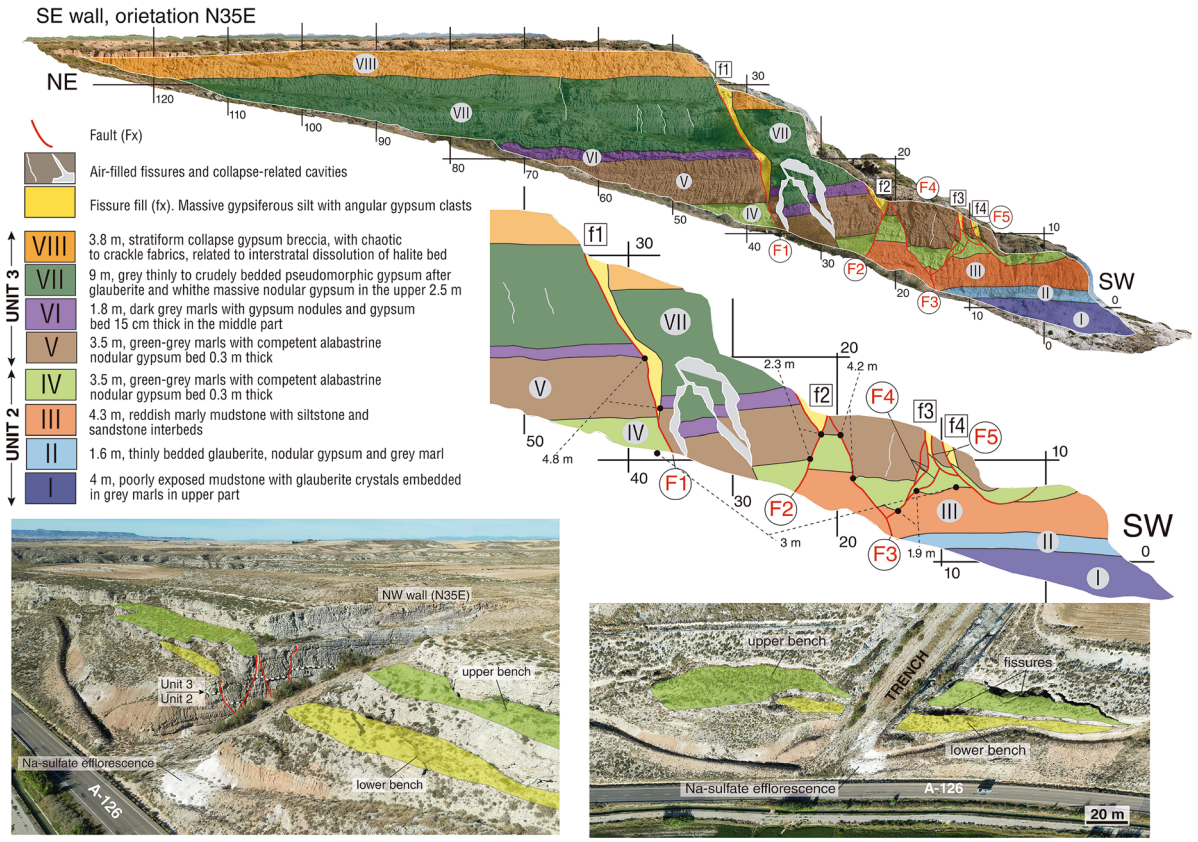

Fig. 9 Log of the SE wall of the megatrench, description of the stratigraphic units, and annotated oblique and vertical images of the trench site. The oblique view shows the NW wall of the trench, with a similar structure to that of the opposite side

between fluvial undercutting and landsliding is also supported by the average distance of the landslides to the river channel, with a value of 501 m for the inactive slope movements, versus 184 m for the active and partially active ones. This indicates a strong spatial and temporal relationship between the dynamics of the fluvial system and the escarpment, with periods of enhanced landslide activity when the river channel is associated with the foot of the scarp (i.e., slope-channel coupling), and phases of attenuated activity or stabilization when the river migrates away for the scarp at each site. This general concept whereby fluvial migration toward the foot of the scarp induces landsliding and scarp retreat can be invoked to hypothesize that the abandonment of El Castellar village in 1574 was at least partially related to a shift of the Ebro River and the associated geomorphic effects (Figs. 5 and 6). This hypothesis is supported by: (1) the age of a terrace in the Barranco de la Salinas (ca. 1500 AD; Constante et al. 2010a) that provides a minimum bound for the incision phase induced by the migration of the river and the associated relative base-level drop; and (2) the presence of an abandoned channel in the floodplain at significant distance from the valley margin (Fig. 5).

Peña Monné et al. (2021), using imagery dating back to 1927 and georeferenced historical maps from the eighteenth and nineteenth centuries, especially a map produced by De Rodolphe (1746), propose that between 1746 and 1927 the Ebro River experienced a dramatic change in its pattern and sinuosity with significant impact on landslide development. Apparently, by 1746 the Ebro River was a nearly rectilinear channel attached to the foot of the escarpment between the Barranco Casa Pola and Alfocea (sinuosity ca. 1.1). In contrast, the aerial photographs from 1927 show a meandering river similar to that of present day (sinuosity 1.6), with the channel in contact with the escarpment only at specific locations (Fig. 1). On the basis of this paleogeographic reconstruction, the authors propose that fluvial undercutting, landslide activity, scarp retreat and the development of hanging valleys was particularly intense during the second part of the Little Ice Age (18th–nineteenth centuries), and that it is currently in a state of relative stability. An alternative explanation, which in our opinion is more reasonable, is that the schematic map by De Rodolphe (1746) does not represent reliably the position and pattern of the meandering channel. In fact, this cartographic work was conducted for the construction of the Imperial Canal along the southern margin of the Ebro Valley (Sástago 1796), a project for which the Ebro River path was not particularly important. Our interpretation is supported by: (1) the lack of geomorphic evidence of a former channel running all along the foot of the escarpment; and (2) the dense network of historical and pre-historical meander loops that occur in the floodplain, indicating that the channel has had a meandering pattern over millennia, interacting with the scarp at specific and variable locations.

In the long term, slope movements fostered by fluvial undercutting plus the erosion of the landslide deposits lead to the recession

of the escarpment. The scarp retreat implies a relative base-level drop for the drainages that debouch at the valley margin, which tend to downcut into the bedrock to maintain a longitudinal profile graded with the Ebro River valley floor. Low-order drainages with small contributing areas and limited incision capability eventually may become hanging valleys (i.e., scarp retreat overwhelms the incision capability). In the study area, 23 hanging valleys out of 31 occur east of Alfocea, where that scarp is entirely made up of a thick gypsum package (Fig. 1). Here, the high density of hanging valleys can be attributed to the following: (1) the lack of easily erodible mudstones and marls, retarding incision rates; and (2) the limited height of the scarp, favoring faster retreat rates. The formation of the other type of perched valleys, namely beheaded valleys, mainly occur in sections where trunk tributary drainages have an oblique orientation with respect to the escarpment. These catchments include low-order valleys that drain away from the escarpment, which headwaters may have been truncated by the recession of the cliff (Fig. 1).

The common occurrence of prominent escarpments with hanging valleys and triangular facets in fluvial valleys carved in gypsum bedrock indicates that these gypsum cliffs tend to experience very rapid retreat (De Waele and Gutiérrez 2022 and references therein). The fast recession of the scarps mainly made up of highly soluble gypsum can be attributed to the combined effect of the following processes:

- Long-term entrenchment of the fluvial system, as is the case of the Ebro River, with terraces perched 235 m above the channel (Gutiérrez et al. 2015).
- Rapid undercutting of the cliff by solutional and mechanical erosion. Navas (1988), in her study on the contribution of gypsum dissolution to the salinization of the surface water in the Ebro River basin, estimated retreat rates by dissolution at the base of gypsum cliffs caused by river waters (i.e., channel in contact with the scarp). She obtained an average solutional recession rate of 0.45 m/year from ten sections of the Ebro River abutting gypsum escarpments. The estimations were obtained using gypsum dissolution kinetics equations that account for the hydrochemistry and hydraulics of the river water, the contact surface, and lithological variables. Navas (1988) estimated that the input of dissolved and detrital gypsum (e.g., rock falls) from gypsum scarps in contact with undermining rivers represents around 11% of the dissolved gypsum in the Ebro River at its mouth.
- Loss of basal support related to subsurface dissolution, preferentially acting along more soluble beds (e.g., halite). As reviewed in the introduction, this subsurface solutional undermining process reduces the mechanical strength of the overlying rocks, and may also contribute to their displacement with a dominant vertical component. It should be noted that scarp retreat involves the addition of new soluble bedrock beneath the expanding floodplain (i.e., groundwater discharge area), inducing renewed dissolution at the foot of the cliff.
- Frequent occurrence of slope movements favored by the limited mechanical resistance of the gypsum and the destabilizing effects of fluvial undercutting, subsurface solutional undermining, and dissolution along discontinuity planes (e.g., joints, unloading cracks). Additionally, the circulation of water in the karst conduit network, especially when the incoming flow exceeds the outflow capacity, may induce high fluid pressures reducing the normal effective stress and the shear strength of potential failure planes.
- Prompt removal of the landslide deposits by chemical and mechanical erosion by river waters, leading to continuous relief rejuvenation. Landslide deposits accumulated at the foot of scarped slopes tend to act as a stabilizing and protecting buttress. However, these protective elements when associated with a river tend to have a very limited persistence time given the highly soluble nature of gypsum (James et al. 1981; Navas 1990).

Multiple lines of evidence indicate that subsurface solutional undermining related to interstratal dissolution of salt units (halite and glauberite) at the basal part of the escarpment plays a preparatory role for the development of landslides, weakening the rock mass by supra-salt gravitational deformation:

- The halite beds ca. 9 m and 3 m thick of units 3 and 4, respectively, pinch out toward the face of the cliff grading into a thin dissolution residue. The interstratal dissolution of the salt by the migration of a dissolution front invariably entails the subsidence of the overlying rocks and their weakening by gravitational deformation. A similar process may also occur by dissolution of glauberite in units 2 and 3, especially where rapid scarp retreat prevents its full transformation into gypsum (incongruent dissolution), as revealed by collapse structures observed in the trench.
- There is a clear spatial association between the slope collapses controlled by nearly vertical failure planes developed close to the scarp face and the sections of the escarpment with halite and glauberite beds at the base of the cliff.
- Extensive efflorescences and other precipitates of halite and Na-sulfates provide evidence of ongoing subsurface dissolution at multiple sites at the base of the cliff.
- The investigated trench displays foundered fault blocks associated with the face of the escarpment with no or negligible vertical offset across the grabens. This fact, together with the lack of back-tilting and internal deformation in the sediments situated in the frontal part of the deformation zone, indicates that the structures are essentially related to a vertical collapse process induced by subjacent glauberite dissolution. Similar features were documented by Tsui and Cruden (1984) in the Salt River gypsum escarpment (Wood Buffalo National Park, Northwest Territories, Canada), formed by horizontally lying Devonian gypsum capped by carbonate rocks. Here, they observed a series of valleyward-stepping fault blocks bounded by steep normal faults associated with the cliff. They attributed these downthrown blocks expressed as rock terraces to differential interstratal gypsum dissolution and the foundering of the overlying carbonate caprock (i.e., collapsed blocks).

Figure 10 proposes an evolutionary model integrating the role played by fluvial undercutting and subsurface solutional undermining in the development of rock-slope collapses. In a relatively stable scarp situated at some distance from the river channel, glauberite has been transformed into gypsum, and halite beds have been dissolved, causing the subsidence and weakening of the overlying

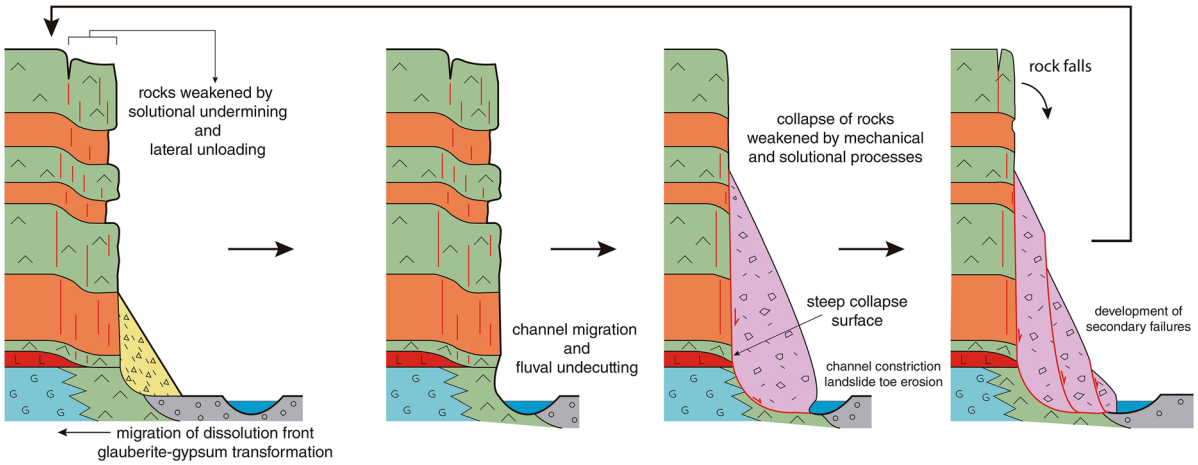

Fig. 10 Evolutionary model integrating the role played by fluvial undercutting and subsurface solutional undermining in the development of slope collapses. See explanation in the text

strata. When the river channel shifts to the base of the escarpment, fluvial undercutting triggers slope collapses with steeply diping failures mainly affecting the rocks associated with the face of the cliff, weakened by solutional undermining and unloading. The debuttressing effect of fluvial erosion at the toe of the landslide deposit can induce internal reactivations. Rapid erosion of the landslide deposit and the bedrock by fluvial erosion (or artificial excavation) may even expose fresh halite and glauberite beds (Fig. 3D).

Conclusions

The lithostratigraphy of the gypsum escarpment controls the distribution and failure mechanism of the inventoried landslides. Rotational landslides occur in sections where the base of the scarp includes mudstones and marls, and the larger ones are associated with the stretch of the cliff with higher local relief, controlled by a resistant limestone caprock. Massive short-runout rock-falls with nearly vertical failure planes, here designated as slope collapses, mainly occur in the section of the escarpment with halite and glauberite beds at the base. This spatial association supports the concept whereby interstratal salt dissolution near the face of the scar and the consequent weakening of the overlying strata by gravitational deformation plays a preparatory role for the development of these landslides. Relatively small rockfalls and topples dominate where the cliff is entirely made up of gypsum.

The geomorphological strip map produced reveals that fluvial undercutting by the mobile meandering Ebro River is the main triggering factor for the occurrence and reactivation of landslides. Geomorphic and chronological evidence supports the hypothesis whereby the abandonment of the El Castellar village was at least partially related to a shift of the river to the foot of the escarpment and the instigation of landslide activity.

Two types of perched valleys have been mapped in the Remolinos escarpment; hanging valleys and beheaded valleys in drainages directed toward and away from the scarp, respectively. The common association of perched valleys with gypsums escarpments at the margin of fluvial valleys reveals that these cliffs can experience very rapid retreat, overwhelming the incision capability of small tributary drainages. The main factors that explain these features are related to two intrinsic characteristics of gypsum rock, including its relatively low mechanical strength and its high solubility. Landslides of various types are easily induced by fluvial undermining, and the landslide deposits are rapidly removed by solutional and mechanical erosion, facilitating further landsliding and scarp recession.

Interstratal dissolution of salt at the base of the cliff plays a preparatory role for landslide development in the Remolinos escarpment, inducing its downward displacement (subsidence) and mechanical weakening. Evidence for this subsurface solutional undermining process includes: (1) spatial association between slope collapses and the section of the escarpment with halite beds at its base; (2) pinching out of halite beds 9 m and 3 m toward the scarp, grading into a dissolution residue overlain by deformed strata; (3) collapsed fault blocks with no or negligible throw across the grabens related to subjacent glauberite dissolution; and (4) brine seepages and extensive efflorescences and other precipitates of Na-sulfate and glauberite.

Acknowledgements

Authors are very grateful to Mike Crozier for his insightful comments on the landslide classification and to the City Hall of Torres de Berrellén for logistic support. This work was supported by projects (CGL2017-85045-P, PID2021-123189NB-I00) of the Spanish Government (Ministerio de Ciencia e Innovación). Participation of P.M. was financially supported by the Bekker Programme Fellowship awarded by the Polish National Agency for Academic Exchange (contract no. PPN/BEK/2020/1/00047/U/DRAFT/00001). J.S. has a predoctoral contract (PRE2018-084240) cofinanced by the Spanish Government and the European Social Fund (ESF).

Author contribution

All authors contributed to the study conception and design. Material preparation, data collection and analysis were performed by all authors. The first draft of the manuscript was written by Francisco Gutiérrez and all authors commented on previous versions of the manuscript. All authors read and approved the final manuscript.

Funding

Open Access funding provided thanks to the CRUE-CSIC agreement with Springer Nature.

Data availability

Data available upon request.

Declarations

Competing interests The authors declare no competing interests.

References

Alberto W, Giardino M, Martinotti G, Tiranti D (2008) Geomorphological hazards related to deep dissolution phenomena in the Western Italian Alps: distribution, assessment and interaction with human activities. Eng Geol 99:147–159. https://doi.org/10.1016/j.enggeo.2007.11.016

Andrejchuk VN, Klimchouk AB (2002) Mechanisms of karst breakdown formation in the gypsum karst of the fore-Ural region, Russia (from observations in the Kungurskaja Cave). Intern J Speleol 31:89–114. https://doi.org/10.5038/1827-806X.31.1.5

Anson R, Hawkins A (2002) Movement of the Soper's Wood landslide on the Jurassic Fuller's Earth, Bath, England. Bull Eng Geol Environ 61:325–345. https://doi.org/10.1007/s10064-002-0151-8

Balasch JC, Pino D, Ruiz-Bellet JL, Tuset J, Barriendos M, Castelltort X, Peña JC (2019) The extreme floods in the Ebro River basin since 1600 CE. Sci Total Environ 646:645–660. https://doi.org/10.1016/j.scitotenv.2018.07.325

Calvo M (2001) Las minas de sal de Remolinos. Revista de Minerales 2:3–22

Carbonel D, Gutiérrez F, Linares R, Roqué C, Zarroca M, McCalpin J, Guerrero J, Rodríguez V (2013) Differentiating between gravitational and tectonic faults by means of geomorphological mapping, trenching and geophysical surveys. The case of the Zenzano Fault (Iberian Chain, N Spain). Geomorphology 189:93–108. https://doi.org/10.1016/j.geomorph.2013.01.020

Chigira M, Wu X, Inokuchi T, Wang G (2010) Landslides induced by the 2008 Wenchuan earthquake, Sichuan, China. Geomorphology 118:225–238. https://doi.org/10.1016/j.geomorph.2010.01.003

Cianflone G, Tolomei C, Brunori CA, Monna S, Dominici R (2018) Landslides and subsidence assessment in the Crati Valley (Southern Italy) using InSAR data. Geosciences 8:67. https://doi.org/10.3390/geosciences8020067

Constante A, Peña-Monné JL, Muñoz A (2010a) Alluvial geoarcheology of an ephemeral stream: implications for Holocene landscape change in the central part of the Ebro Depression, Northeast Spain. Geoarchaeology 25:475–496. https://doi.org/10.1002/gea.20314

Constante A, Peña-Monné JL, Muñoz A, Picazo J (2010b) Climate and anthropogenic factors affecting alluvial fan development during the late Holocene in the central Ebro Valley, northeast Spain. Holocene 21:275–286. https://doi.org/10.1177/0959683610378

Cuadrat JM, Saz MA, Vicente SM (2007) Atlas Climático de Aragón. Gobierno de Aragón, Zaragoza, p 222

De Waele J, Gutiérrez F (2022) Karst hydrogeology, geomorphology and caves. Wiley, Chichester, p 888

Denchik N, Gautier S, Dupuy M, Batiot-Guilhe C, Lopez M, Léonardi V, Geeraert M, Henry G, Neyens D, Coudray P, Pezard PA (2019) In-situ geophysical and hydro-geochemical monitoring to infer landslide dynamics (Pégairolles-de-l'Escalette landslide, France). Eng Geol 254:102–112. https://doi.org/10.1016/j.enggeo.2019.04.009

El-Haddad BA, Youssef AM, El-Shater AH, El-Khashab MH (2021) Landslide mechanisms along carbonate rock cliffs and their impact on sustainable development: a case study. Egypt Arab J Geosci 14:1–14. https://doi.org/10.1007/s12517-021-06688-1

García-Veigas J, Ortí F, Fernández-Nieto C (1994) Modelo hidroquímico de sedimentación de glauberita-halita: sondeo PURASAL, Formación Yesos de Zaragoza (Mioceno inferior, Cuenca del Ebro). Geogaceta 16:136–139

Gascón Ricao A (2007) El hechizo de El Castellar. Cuadernos de Aragón 35:144

Gökkaya E, Gutiérrez F, Ferk M, Görüm T (2021) Sinkhole development in the Sivas gypsum karst. Turkey. Geomorphology 386:107746. https://doi.org/10.1016/j.geomorph.2021.107746

Guerrero J, Gutiérrez F (2017) Gypsum scarps and asymmetric fluvial valleys in evaporitic terrains. The role of river migration, landslides, karstification and lithology (Ebro River, NE Spain). Geomorphology 297:137–152. https://doi.org/10.1016/j.geomorph.2017.09.018

Guglielmi Y, Bertrand C, Compagnon F, Follacci JP, Mudry J (2000) Acquisition of water chemistry in a mobile fissured basement massif: its role in the hydrogeological knowledge of the La Clapiere landslide (Mercantour massif, southern Alps, France). J Hydrol 229:138–148. https://doi.org/10.1016/S0022-1694(00)00166-9

Gutiérrez F, Arauzo F, Desir G (1994) Deslizamientos en el escarpe en yesos de Alfajarín (Zaragoza). Cuaternario y Geomorfología 8:57–68

Gutiérrez F, Benito-Calvo A, Carbonel D, Desir G, Sevil J, Guerrero J, Martínez-Fernández A, Karampaglidis T, García-Arnay A, Fabregat I (2019) Review on sinkhole monitoring and performance of remediation measures by high-precision leveling and terrestrial laser scanner in the salt karst of the Ebro Valley, Spain. Eng Geol 248:283–308. https://doi.org/10.1016/j.enggeo.2018.12.004

Gutiérrez F, Calaforra JM, Cardona F, Ortí F, Durán JJ, Garay P (2008) Geological and environmental implications of the evaporite karst in Spain. Environ Geol 53:951–965. https://doi.org/10.1007/s00254-007-0721-y

Gutiérrez F, Galve JP, Guerrero J, Lucha P, Cendrero A, Remondo J, Bonachea J, Gutiérrez M, Sánchez JA (2007) The origin, typology, spatial distribution, and detrimental effects of the sinkholes developed in the alluvial evaporite karst of the Ebro River valley downstream Zaragoza city (NE Spain). Earth Surf Proc Landf 32:912–928. https://doi.org/10.1002/esp.1456

Gutiérrez F, Linares R, Roqué C, Zarroca M, Carbonel D, Rosell J, Gutiérrez M (2015) Large landslides associated with a diapiric fold in Canelles Reservoir (Spanish Pyrenees): detailed geological-geomorphological mapping, trenching and electrical resistivity imaging. Geomorphology 241:224–242. https://doi.org/10.1016/j.geomorph.2015.04.016

Gutiérrez F, Linares R, Roqué C, Zarroca M, Rosell J, Galve JP, Carbonel D (2012) Investigating gravitational grabens related to lateral spreading and evaporite dissolution subsidence by means of detailed mapping, trenching, and electrical resistivity tomography (Spanish Pyrenees). Lithosphere 4:331–353. https://doi.org/10.1130/L202.1

Gutiérrez F, Lucha P, Galve JP (2010) Reconstructing the geochronological evolution of large landslides by means of the trenching technique in the Yesa Reservoir (Spanish Pyrenees). Geomorphology 124:124–136. https://doi.org/10.1016/j.geomorph.2010.04.015

Ibáñez MJ, Mensua S (1976) Contribución al estudio de vertientes en condiciones semiáridas: Tipos de vertientes sobre yesos en el valle del Ebro. Boletín Real Soc Geogr 112:381–391

Jaboyedoff M, Crosta GB, Stead D (2011) Slope tectonics: a short introduction. Geol Soc London, Spec Publ 351:1–10. https://doi.org/10.1144/SP351.1
James AN, Cooper AH, Holliday DW (1981) Solution of the gypsum cliff (Permian, Middle Marl) by the River Ure at Ripon Parks, North Yorkshire. Proc Yorkshire Geol Soc 43:433–450. https://doi.org/10.1144/pygs.43.4.433
Mateos RM, Ezquerro P, Azañón JM, Gelabert B, Herrera G, Fernández-Merodo JA, Spizzichino ID, Sarro R, García-Moreno I, Béjar-Pizarro M (2018) Coastal lateral spreading in the world heritage site of the Tramuntana Range (Majorca, Spain). The use of PSInSAR monitoring to identify vulnerability. Landslides 15:797–809. https://doi.org/10.1007/s10346-018-0949-5
McCalpin JP (2013) Trenching and exposed faces. In: Shroder J (Ed in Chief), Switzer A, Kennedy DM (eds) Treatise on Geomorphology, vol 14, Methods in Geomorphology. Academic Press, San Diego, CA, pp 138–149. https://doi.org/10.1016/B978-0-12-374739-6.00379-1
Navas A (1988) La participación de los yesos en la salinización de las aguas superficiales de la Cuenca del Ebro. PhD Thesis. University of Zaragoza, p 466
Navas A (1990) The effect of hydrochemical factors on the dissolution rate of gypsiferous rocks in flowing water. Earth Surf Proc Landf 15:709–715. https://doi.org/10.1002/esp.3290150805
Ollero A (2010) Channel changes and floodplain management in the meandering middle Ebro River, Spain. Geomorphology 117:247–260. https://doi.org/10.1016/j.geomorph.2009.01.015
Ordóñez S (2022) Geología de la unidad salina de la Cuenca de Madrid. Recursos minerales, riesgosgeológicos y mineralogénesis salina. Bol Real Soc Esp Hist Nat 116:5–23
Pardo G, Arenas C, González A, Luzón A, Muñoz A, Pérez A, Pérez-Riverés FJ, Vázquez-Urbez M, Villena J (2004) La Cuenca del Ebro. In: Vera JA (ed) Geología de España. SGE-IGME, pp 533–542
Pellicer F, Echevarría MT, Ibáñez MJ (1984) Procesos actuales en el escarpe de yesos de Remolinos. Cuadernos De Investigación Geográfica 10:159–169
Pellicer F, Yetano LM (1985) El galacho de Juslibol: un ejemplo de meandro abandonado. Cuadernos De Investigación Geográfica 11:113–124
Peña-Monné JL, Sampietro-Vattuone MM, Longares-Añadrén LA, Sánchez-Fabre M, Constante A (2021) Interactions between fluvial dynamics and scarp retreat in the Central Ebro Basin during MCA and LIA periods: Paleogeographical and geoarchaeological reconstruction. Paleogeogr Paleoclimatol Paleoecol 567:110301. https://doi.org/10.1016/j.palaeo.2021.110301
Pérez-Rivarés FJ, Arenas C, Pardo G, Garcés M (2018) Temporal aspects of genetic stratigraphic units in continental sedimentary basins: examples from the Ebro basin, Spain. Earth Sci Rev 178:136–153. https://doi.org/10.1016/j.earscirev.2018.01.019
Pérez-Rivarés FJ, Garcés M, Arenas C, Pardo G (2004) Magnetostratigraphy of the Miocene continental deposits of the Montes de Castejón (central Ebro basin, Spain): geochronological and paleoenvironmental implications. Geol Acta 2:221–234. https://doi.org/10.1344/105.000001429
Quirantes J (1978) Estudio sedimentológico y estratigráfico del Terciario contniental de Los Monegros. Institución Fernando El Católico, Diputación Provincial de Zaragoza, Zaragoza, p 200
Regato P (1988) Contribución al estudio de la flora y la vegetación del Galacho de La Alfranca en relación con la evolución del sistema fluvial. Naturaleza en Aragón. DGA, Zaragoza, p 189
Reuter F, Molek H, Bochmann G (1977) Slope sliding as secondary process in subsidence areas of chloride-karst. Bull Intern Assoc Eng Geol 16:62–64. https://doi.org/10.1007/BF02591448
Rovéra G (1993) Instabilité des versants et dissolution des évaporites dans les Alpes internes: l'exemple de la montagne de Friolin (Peisey-Nancroix, Savoie). Rev Géogr Alpine 81:71–84. https://doi.org/10.3406/rga.1993.3696
Salvany JM (2009) Geologia del yacimiento glauberitico de Montes de Torrero. Universidad de Zaragoza, Zaragoza, p 80
Salvany JM, Garcia-Veigas J, Ortí F (2007) Glauberite-halite association of the Zaragoza Gypsum Formation (lower Miocene, Ebro Basin, NE Spain). Sedimentology 54:443–467. https://doi.org/10.1111/j.1365-3091.2006.00844.x
Sástago C (1796) Descripción de los Canales Imperial de Aragón y Real de Tauste. Ministerio de Fomento, Madrid, p 174
Seijmonsbergen AC, de Graff LWS (2006) Geomorphological mapping and geophysical profiling for the evaluation of natural hazards in an alpine catchment. Nat Haz Earth Syst Sci 6:185–193. https://doi.org/10.5194/nhess-6-185-2006
Silva P, Goy JL, Zazo C (1988) Neotectónica en el sector centro-meridional de la Cuenca de Madrid. Estudios Geol 44:415–427. https://doi.org/10.3989/egeol.88445-6558
Torrescusa S, Klimowitz J (1990) Contribución al conocimiento de las evaporitas Miocenas (Fm. Zaragoza) de la Cuenca del Ebro. In: Ortí, Salvany JM (eds) Formaciones evaporíticas de la Cuenca del Ebro, cadenas periféricas y de la zona de Levante. Enresa, Barcelona, pp 120–123
Tsui PC, Cruden DM (1984) Deformation associated with gypsum karst in the Salt River Escarpment, northeastern Alberta. Can J Earth Sci 21:949–959. https://doi.org/10.1139/e84-099
Wang X, Xiao Y, Shi W, Ren J, Liang F, Lu J, Li H, Yu X (2022) Forensic analysis and numerical simulation of a catastrophic landslide of dissolved and fractured rock slope subject to underground mining. Landslides 19:1045–1067. https://doi.org/10.1007/s10346-021-01842-y
Warren JK (2016) Evaporites. A geological compendium. Springer, Cham, p 1813
Zhang M, McSaveney M, Shao H, Zhang C (2018) The 2009 Jiweishan rock avalanche, Wulong, China: precursor conditions and factors leading to failure. Eng Geol 233:225–230. https://doi.org/10.1016/j.enggeo.2017.12.010

Francisco Gutiérrez (✉) · Jorge Sevil
Department of Earth Sciences, University of Zaragoza, C/. Pedro Cerbuna 12, 50009 Zaragoza, Spain
Email: fgutier@unizar.es

Piotr Migoń
Institute of Geography and Regional Development, University of Wrocław, Pl. Uniwersytecki 1, 50-137 Wrocław, Poland